*molecules*

MDPI

*Article*

# Schiff Base Compounds Derived from 5-Methyl Salicylaldehyde as Turn-On Fluorescent Probes for $Al^{3+}$ Detection: Experimental and DFT Calculations

**Huan-Qing Li, Shi-Hang Yang, Yun Li, Wan-Xin Ye, Zi-Yu Liao, Jia-Qian Lu and Zhao-Yang Wang ***

School of Chemistry, South China Normal University, Guangzhou Key Laboratory of Analytical Chemistry for Biomedicine, GDMPA Key Laboratory for Process Control and Quality Evaluation of Chiral Pharmaceuticals, Key Laboratory of Theoretical Chemistry of Environment, Ministry of Education, Guangzhou 510006, China; 2022022611@m.scnu.edu.cn (H.-Q.L.); 2024022743@m.scnu.edu.cn (S.-H.Y.); 2024022879@m.scnu.edu.cn (Y.L.); 2024022841@m.scnu.edu.cn (W.-X.Y.); 20212421083@m.scnu.edu.cn (Z.-Y.L.); 20222421008@m.scnu.edu.cn (J.-Q.L.)
* Correspondence: wangzy@scnu.edu.cn; Tel.: +86-020-3931-0258; Fax: +86-020-3931-0187

**Abstract:** Using 5-methyl salicylaldehyde (**2**) as a reactant to react with different amines, 2-aminobenzimidazole (**1a**), 2-aminobenzothiazole (**1b**), and 2-aminopyridine (**1c**), respectively, three types of Schiff base fluorescent probes **3a**–**3c** were designed and synthesized for selective detection of $Al^{3+}$ in aqueous media. The structure of the compounds was acquired by $^{1}H$ NMR, $^{13}C$ NMR, and X-ray single-crystal diffraction. Furthermore, their photochromic and fluorescent behaviors have been investigated systematically by fluorescence spectra. Compounds **3a**–**3c** can exhibit high selectivity, sensitivity, and anti-interference properties towards $Al^{3+}$ in aqueous media. Among them, the limit of detection (LOD) of probe **3b** for $Al^{3+}$ is $2.81 \times 10^{-7}$ M. Notably, the response times of probes **3a**–**3c** for $Al^{3+}$ are 90 s, 80 s, and 80 s, respectively, which are much faster than most previously reported probes. The coordination stoichiometry between compounds **3a**–**3c** and $Al^{3+}$ has been verified to be 1:1 through the Job's plot. After coordination with $Al^{3+}$, the C=N isomerization of compounds **3a**–**3c** is inhibited, leading to the closure of the excited state intramolecular proton transfer (ESIPT) effect. At the same time, the fluorescence intensity is significantly increased through chelation-enhanced fluorescence mechanism (CHEF), which is confirmed by density functional theory (DFT) calculations. In addition, probes **3a**–**3c** can be potentially applied in the selective and high-precision detection of $Al^{3+}$ in environmental systems.

**Keywords:** Schiff base; 5-methyl salicylaldehyde; $Al^{3+}$ fluorescent probe; excited state intramolecular proton transfer; chelation-enhanced fluorescence mechanism; DFT calculations

check for updates

Academic Editor: Panwang Zhou

Received: 7 February 2025
Revised: 23 February 2025
Accepted: 27 February 2025
Published: 28 February 2025

**Citation:** Li, H.-Q.; Yang, S.-H.; Li, Y.; Ye, W.-X.; Liao, Z.-Y.; Lu, J.-Q.; Wang, Z.-Y. Schiff Base Compounds Derived from 5-Methyl Salicylaldehyde as Turn-On Fluorescent Probes for $Al^{3+}$ Detection: Experimental and DFT Calculations. *Molecules* **2025**, *30*, 1128. https://doi.org/10.3390/molecules30051128

**Copyright:** © 2025 by the authors. Licensee MDPI, Basel, Switzerland. This article is an open access article distributed under the terms and conditions of the Creative Commons Attribution (CC BY) license (https://creativecommons.org/licenses/by/4.0/).

## 1. Introduction

It is well known that aluminum is the most abundant metal element in the Earth's crust [1] and is widely used in many fields, such as food packaging, building materials, and electronic devices [2]. Due to the widespread presence of aluminum products in people's daily lives, the harm of aluminum to humans has attracted widespread attention in recent years [3]. $Al^{3+}$ is a neurotoxin and a "silent killer" in the human body [4]. The World Health Organization (WHO) has listed $Al^{3+}$ as a source of food contamination and set the maximum allowable concentration in drinking water at 7.41 μM [5]. Long-term excessive intake of $Al^{3+}$ can lead to major diseases such as Parkinson's disease, Alzheimer's disease, and rickets [6]. In addition, high concentrations of $Al^{3+}$ deposition can lead to soil acidification, which can seriously harm crops and soil ecosystems [7]. Therefore,

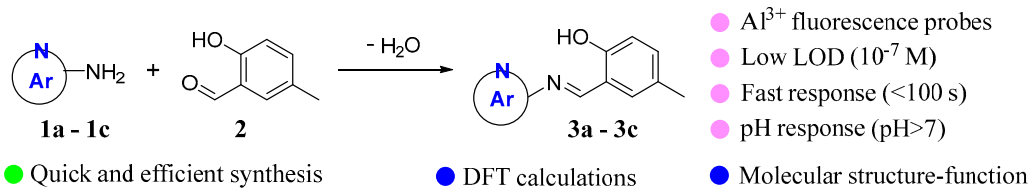
developing a selective and effective method for detecting $Al^{3+}$ is crucial for human health and ecological protection.

Traditional $Al^{3+}$ analysis methods, such as inductively coupled plasma optical emission spectroscopy (ICP OES) [8], atomic absorption spectroscopy (AAS) [9], and capillary electrophoresis (CE) [10], can accurately determine the content of $Al^{3+}$. However, these detection techniques still have many drawbacks, such as complex processes, high detection costs, the need for very professional personnel, and the need for a large number of sample pretreatment [11,12].

In recent years, fluorescence probe detection technology has become an effective method for detecting $Al^{3+}$ due to its simple operation, good selectivity, and real-time detection [13], which has attracted widespread attention from researchers [14,15]. Due to the strong hydration ability of $Al^{3+}$, its coordination with transition metal ions is relatively poor and lacks spectral characteristics. Therefore, many research groups have recently made new breakthroughs in the development of fluorescent probes to address this issue [16–18]. However, some fluorescent probes still have various other problems, including long response times, high detection limits, and poor anti-interference ability [19–21]. Therefore, fluorescence technology for detecting $Al^{3+}$ still poses significant challenges [22].

Considering the Hard Soft Acid Base Theory (HSAB), $Al^{3+}$ is a hard acid that tends to bind to coordination molecules with donor atoms such as N and O to form stable complexes [23,24]. Therefore, most reported $Al^{3+}$ probes contain hard base donor sites, such as N and O atoms [25–27]. Among them, Schiff base compounds are widely used in the development of $Al^{3+}$ fluorescent probes due to their advantages, such as simple synthesis routes, strong metal ion coordination ability, and fast response speed [28–30]. However, the structure-activity relationship of the obtained Schiff base $Al^{3+}$ fluorescent probes based on different nitrogen heterocyclic compounds still needs to be deeply studied, especially the influence of different nitrogen heterocyclic fluorescent groups needs to be explored.

In view of this, based on our previous research on benzazole-based metal ion fluorescent probes [31,32], herein, we further designed three fluorescent probes containing benzimidazole group, benzothiazole group, and pyridine group (Scheme 1). Three Schiff base fluorescent probes **3a**–**3c** were rapidly, efficiently, and environmentally synthesized through a simple one-step Schiff base condensation reaction by using 2-aminobenzimidazole (**1a**), 2-aminobenzothiazole (**1b**), 2-aminopyridine (**1c**), and 5-methyl salicylaldehyde (**2**) as starting materials.




**Scheme 1.** Design of Schiff base probes **3a**–**3c** with nitrogen-containing heterocyclic structure for $Al^{3+}$ detection.

The test results indicate that they can selectively detect $Al^{3+}$ with a low detection limit and fast detection speed. Furthermore, we systematically studied the relationship between the structure and properties of fluorescent groups in Schiff base probes with different nitrogen heterocyclic structures using density functional theory (DFT) calculations, which can provide the guidance for the design and synthesis of novel Schiff base $Al^{3+}$ fluorescent probes.

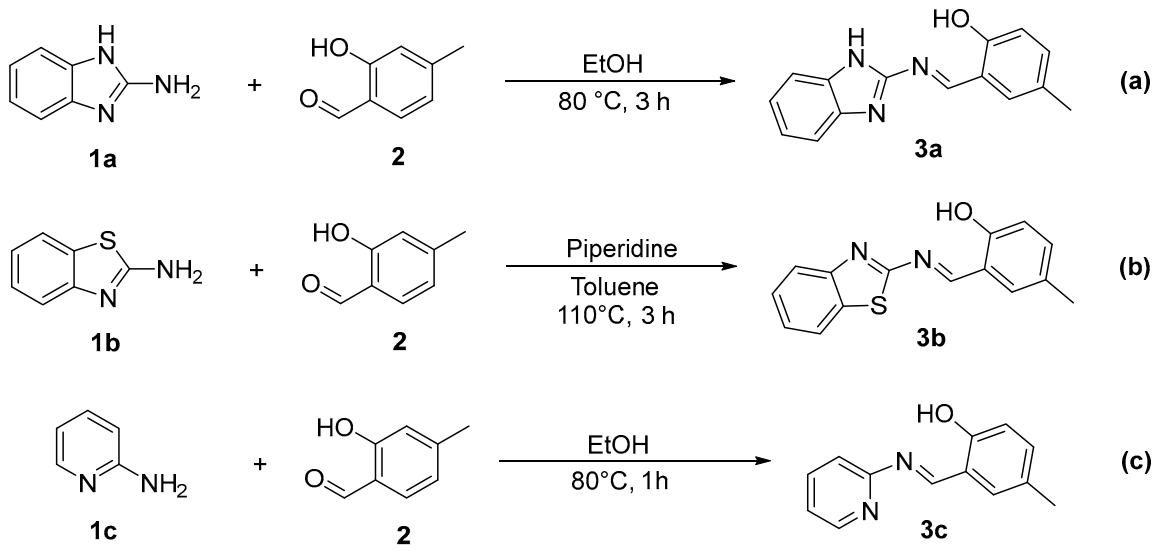
## 2. Results and Discussion

### *2.1. Design, Synthesis, and Structural Characterization of Compounds* **3a–3c**

Salicylaldehyde and its derivatives are commonly found bioactive elements in cosmetics and natural products [33]. They can also be used as raw materials to participate in the construction of conjugated metal–organic frameworks (c-MOF) materials [34], photochromic materials [35], nanomaterials [36], and fluorescent probes [37]. Primarily, due to their excellent photostability and ability to regulate fluorescence properties [38], salicylaldehyde and its derivatives have been widely used as fluorescent probes for detecting cations [39], anions [40], and monitoring pH changes in biological systems [41].

By using the reaction of the aldehyde group, salicylaldehyde often reacts with heterocyclic amine compounds to synthesize Schiff base probe molecules through a one-step Schiff base reaction [39,42]. In addition, the hydroxyl group of salicylaldehyde can also participate in coordination as a proton donor to detect metal ions [43]. The optical properties of Schiff base compounds can be easily adjusted by incorporating different fluorescent groups into their molecular skeleton [25], while *N*-heterocyclic compounds have good fluorescence properties and are often used to synthesize organic small molecule fluorescent probes [44,45]. Therefore, we designed three Schiff base fluorescent probes based on 5-methyl salicylaldehyde by introducing different nitrogen heterocyclic fluorescent groups, respectively.

At present, most Schiff base probe molecules are synthesized using anhydrous ethanol [46] or methanol [47] as solvent. In the synthesis process of compounds **3a–3c**, we found that both compounds **3a** and **3c** can be synthesized by the above method with satisfactory yields. However, when compound **3b** is synthesized using anhydrous ethanol as a solvent, the yield is relatively low. The reason for this may be related to the molecular structure of substrates **1a–1c** (Scheme 2).




**1a** **2** **3a**

**1b** **2** **3b**

**1c** **2** **3c**

**Scheme 2.** (**a**–**c**) Synthetic route of compounds **3a–3c**.

The imidazole structure in **1a** and the pyridine structure in **1c** make the entire molecule more alkaline, except that the substrates all have primary amino groups due to the electron-withdrawing property of benzothiazole, and **1b** can stabilize the conjugated system of the entire molecule, making the alkalinity of **1b** molecule weaker. Therefore, this allows compounds **3a** and **3c** to be synthesized directly in anhydrous ethanol, while the synthesis of compound **3b** requires the addition of piperidine as a catalyst [48].

From the characterization spectra of $^{1}$H NMR and $^{13}$C NMR of the synthesized compounds, it can be observed that compounds **3a**–**3c** can find the corresponding peaks at the expected chemical shifts. In addition, the HRMS and X-ray single crystal diffraction of compound **3a** (Table S1) further confirmed its structure (Figure 1). In a word, various test characterizations indicate that the synthesized compounds **3a**–**3c** are indeed the target compounds, as designed.

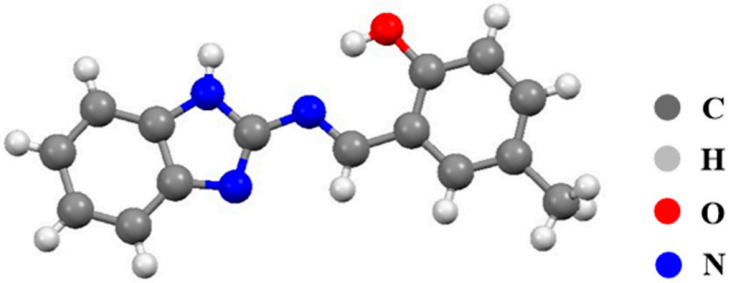



**Figure 1.** Crystal structure of compound **3a**.

### *2.2. Theoretical Calculation Study for Compounds* **3a**–**3c**

As is well known, the excited-state intramolecular proton transfer (ESIPT) refers to the process of transferring protons from proton donor groups to nearby proton acceptor groups after a molecule transitions from the ground state to the excited state [49]. Salicylaldehyde Schiff base derivatives can use phenolic hydroxyl groups as proton donors and nitrogen atoms in imines as proton acceptors, thereby generating significant ESIPT driving forces [50].

Based on this, we designed and synthesized Schiff base probe molecules **3a**–**3c** by using 5-methyl salicylaldehyde (**2**) and nitrogen-containing heterocycles (**1a**–**1c**) as the starting materials. When the probe coordinates with metal ions, the ESIPT effect is turned off, and the fluorescence of the probe changes, making it suitable for detecting metal ions. Compounds with the ESIPT effect often have ketone and enol isomers [49]. To demonstrate the ESIPT effect of probes **3a**–**3c**, we calculated the highest occupied molecular orbital (HOMO) and the lowest unoccupied molecular orbital (LUMO) energies of the enol and ketone isomers of probes **3a**–**3c**.

Based on the Gaussian 09 program D.01, time-dependent DFT (TD-DFT) calculations were performed on these synthesized compounds **3a**–**3c** and their keto tautomers by using the B3LYP/6-31G(d,p) basis set, following the method described in references [51,52]. The aim is to analyze the relationship between structure and photophysical properties, as well as to investigate the ESIPT properties of compounds **3a**–**3c** [53]. The optimized molecular structures and their corresponding frontier molecular orbitals are shown in Figures 2 and 3 (enol form) and Figures 4 and 5 (ketone form), respectively.

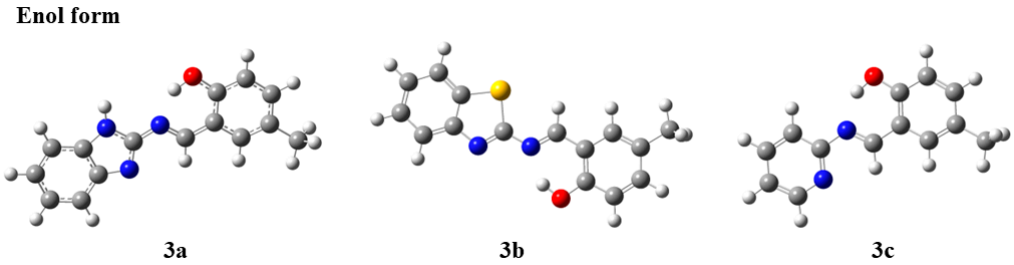



**Figure 2.** Optimized molecular structures of compounds **3a**–**3c** (enol form).

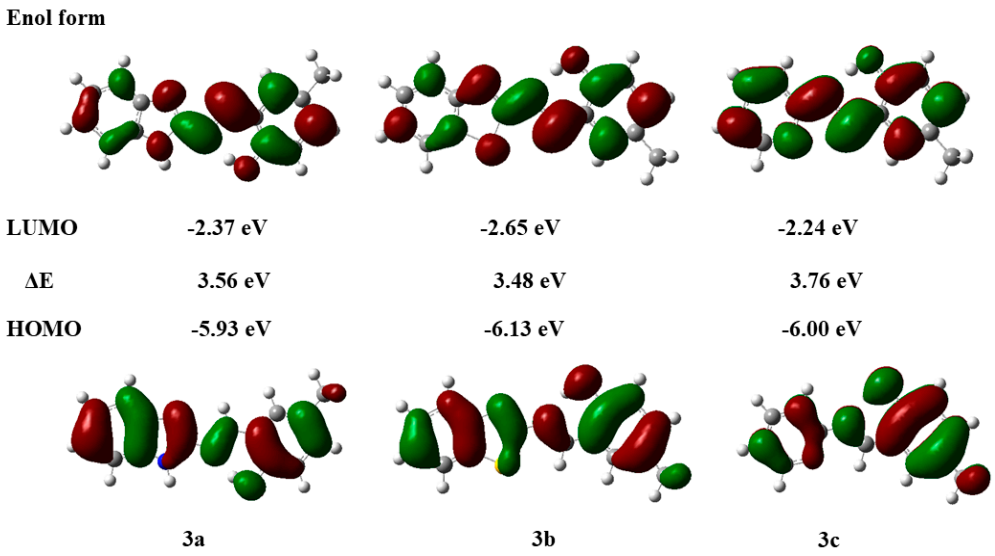



**Figure 3.** Frontline molecular orbitals and energy levels of compounds **3a**–**3c** (enol form).

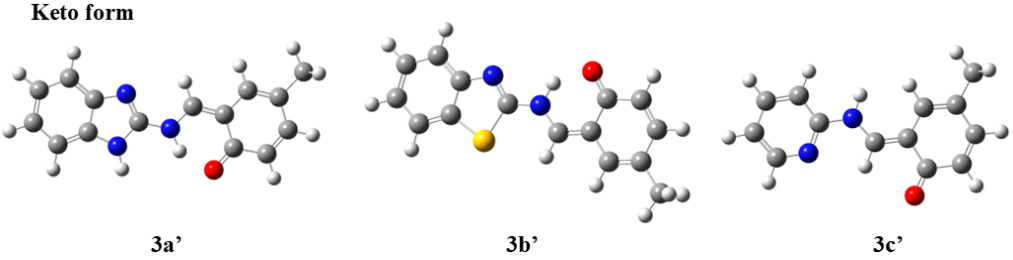



**Figure 4.** Optimized molecular structures of compounds **3a′**–**3c′** (keto form).

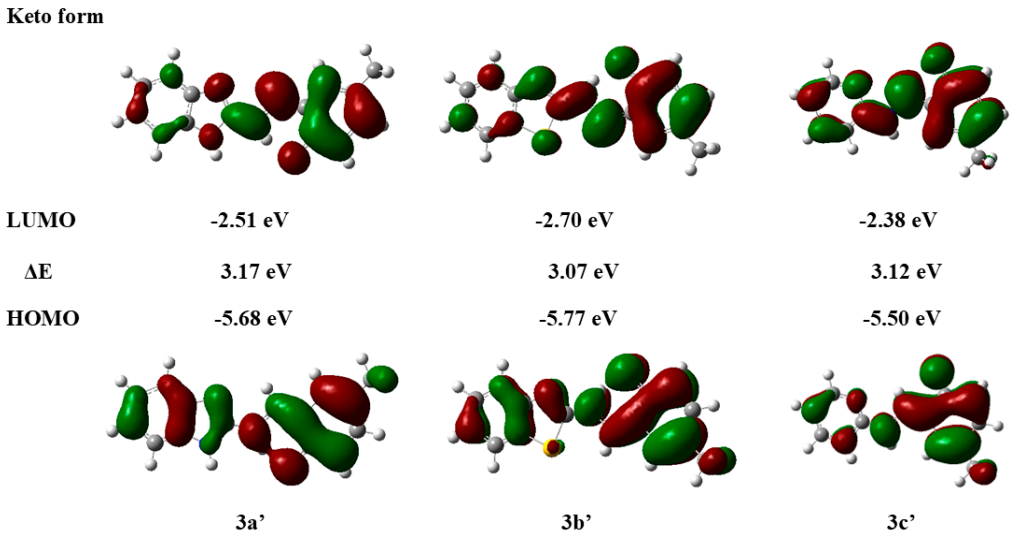



**Figure 5.** Frontline molecular orbitals and energy levels of compounds **3a′**–**3c′** (keto form).

After geometry structural optimization, all compounds **3a**–**3c** exhibit near-planar structure, as shown in Figure 2, which is favorable for molecular aggregation. Meanwhile, as shown in Figure 3, there is a large steric overlap between the HOMO and LUMO of compounds **3a**–**3c**, which are widely distributed throughout the probe molecule. This indicates the good fluorescence properties of probes. However, the fast isomerization around the C=N bond weakens the fluorescence properties of compounds **3a**–**3c**, which may be attributed to their ESIPT process [39].

As shown in Figure 4, the optimized geometric structures of the ketone isomers of compounds **3a**–**3c** still exhibit near-planar structure. Furthermore, we calculated the energy states generated by the HOMO and LUMO orbitals of the ketone isomers of compounds **3a**–**3c** (Figure 5). It can be seen that the LUMO energy level of the enol isomers is higher than that of the ketone isomers. Therefore, the enol isomers are unstable in the excited state, and the phenolic hydroxyl proton will transfer to the nitrogen atom of the Schiff base, forming ketone isomers. Meanwhile, the energy gaps of the ketone isomers of compounds **3a**–**3c** ($\Delta E'_{3a}$ = 3.17 eV, $\Delta E'_{3b}$ = 3.07 eV, $\Delta E'_{3c}$ = 3.12 eV) are smaller than those of the enol isomers ($\Delta E_{3a}$ = 3.56 eV, $\Delta E_{3b}$ = 3.48 eV, $\Delta E_{3c}$ = 3.76 eV), laying the foundation for the formation of ESIPT effect [44].

### *2.3. Study on the Optical Properties of Compounds* **3a**–**3c**

#### 2.3.1. Study on the Optical Properties of Compounds **3a**–**3c** in Different Solvents

To better investigate the performance of probes, we studied the fluorescence emission spectra of compounds **3a**–**3c** in different solvents (Figure S1). It can be seen that the compound has two emission peaks in lower polarity solvents (DCM, EA) for all three probes, belonging to the enol/ketone form, which is consistent with the ESIPT effect [54], and it is obvious that, in DMF, there is the best fluorescence signal. Therefore, in order to obtain a better luminescence intensity while taking into account the solubility problem, we chose to observe the fluorescence detection ability of compounds **3a**–**3c** in DMF.

#### 2.3.2. Study on the ACQ Properties of Compounds **3a**–**3c**

We studied the fluorescence properties of compounds **3a**–**3c** in solvent systems of DMF and water at different ratios using fluorescence emission spectroscopy. The fluorescence spectra are shown in Figures S2 and S3 and Figure 6. The compounds **3a**–**3c** have similar structures, and their fluorescence emission peaks exhibit the same trend in solvent systems of DMF and water at different ratios.

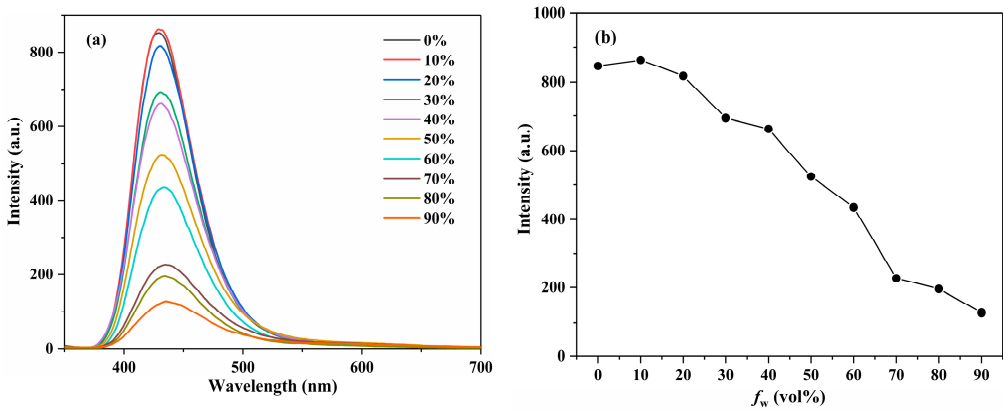



**Figure 6.** (**a**) The fluorescence spectra of compound **3c** (10 μM) and (**b**) the plot of emission peak intensity in DMF/$H_2O$ systems with different water fractions (0–90% by volume).

It can be seen that compared with pure DMF solution, the fluorescence emission peak slightly red-shifts when water is added, and the fluorescence intensity is highest when the water ratio is 10%. Then, as the water ratio continues to increase, the fluorescence intensity decreases significantly. This may be due to the aggregation of compounds with increasing water ratio, resulting in an aggregation-caused quenching (ACQ) effect [55] and a decrease in fluorescence intensity.

Based on the above analysis, a DMF/$H_2O$ solvent system with a water content of 10% was selected for the subsequent performance research experiments.

### *2.4. Research on the Detection of Metal Ions with Compounds* **3a–3c**

#### 2.4.1. Selective Study of Compounds **3a–3c** with Metal Ions

The fluorescence emission spectra of compounds **3a–3c** (10 μM) and different metal ions (100 μM) were studied in a solvent system of DMF/$H_2O$ ($v/v$ = 9:1), including $Al^{3+}$, $K^+$, $Na^+$, $Mg^{2+}$, $Ca^{2+}$, $Zn^{2+}$, $Cu^{2+}$, $Mn^{2+}$, $Co^{2+}$, $Cr^{3+}$, $Hg^{2+}$, $Cd^{2+}$, $Ni^{2+}$, $Pb^{2+}$, $Fe^{2+}$, and $Fe^{3+}$. The fluorescence spectra are shown in Figure 7.

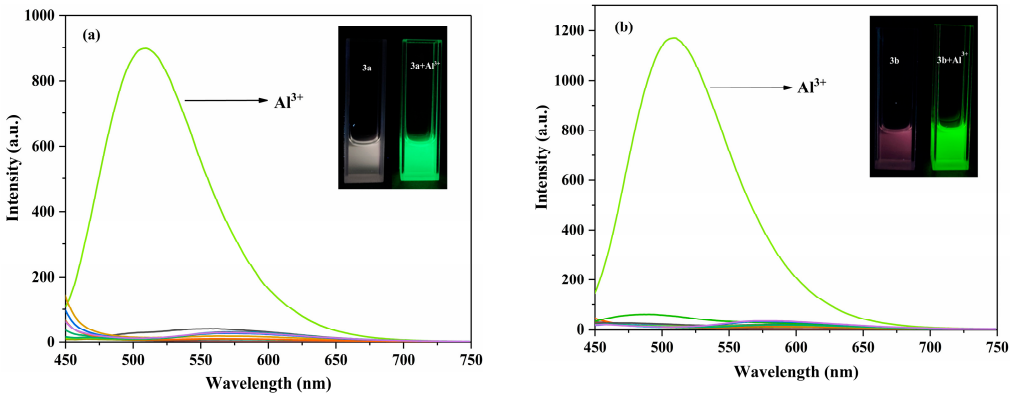



**Figure 7.** Fluorescence spectra of probe **3a** (**a**) and **3b** (**b**) (10 μM) with various metal ions in DMF/$H_2O$ ($v/v$ = 9:1) ($\lambda_{ex}$ = 405 nm for **3a** and $\lambda_{ex}$ = 400 nm for **3b**).

It can be observed that adding $Al^{3+}$ to the solution of compound **3a** enhances the fluorescence intensity of the emission peak at 508 nm, changing from weak light-yellow fluorescence to yellow-green fluorescence (Figure 7a). Similarly, adding $Al^{3+}$ to the solution of compound **3b** enhances the fluorescence intensity at 509 nm, changing from weak light red fluorescence to strong yellow-green fluorescence (Figure 7b). These may be attributed to the coordination of compounds **3a** and **3b** with $Al^{3+}$, further enhancing their structural rigidity and inhibiting ESIPT and C=N isomerization processes. In addition, the fluorescence response of compounds **3a** and **3b** to other metal ions is almost negligible. Compared with blank probes, the test results indicate that both **3a** and **3b** can serve as a specific "turn-on" probe for $Al^{3+}$.

Differently, both the addition of $Al^{3+}$ and $Zn^{2+}$ to compound **3c** solution can enhance the fluorescence emission peak. Among them, the addition of $Al^{3+}$ causes the solution to change from light purple fluorescence to yellow-green fluorescence while adding $Zn^{2+}$ causes the solution to turn yellow fluorescence, and the fluorescence enhancement is more significant (Figure S4). Of course, the fluorescence response of compound **3c** to other metal ions is almost negligible, also indicating that compound **3c** can serve as a specific "turn-on" probe for $Al^{3+}$ and $Zn^{2+}$.

#### 2.4.2. Anti-Interference Study of Compounds **3a–3c** with Metal Ions

In order to further evaluate the selectivity of compounds **3a–3c** towards target ions, competitive experiments were conducted in a solvent system of DMF/$H_2O$ ($v/v$ = 9:1) to investigate the anti-interference of compounds **3a–3c**.

From Figure 8, it can be seen that the fluorescence is enhanced when $Al^{3+}$ is added to compounds **3a** (Figure 8a) and **3b** (Figure 8b). On the contrary, the fluorescence intensity of the solution does not change significantly when other metal ions are added. However, after continuing to add $Al^{3+}$, the fluorescence is enhanced. These indicate that most metal ions do not significantly interfere with the detection of $Al^{3+}$ for compounds **3a** and **3b**.

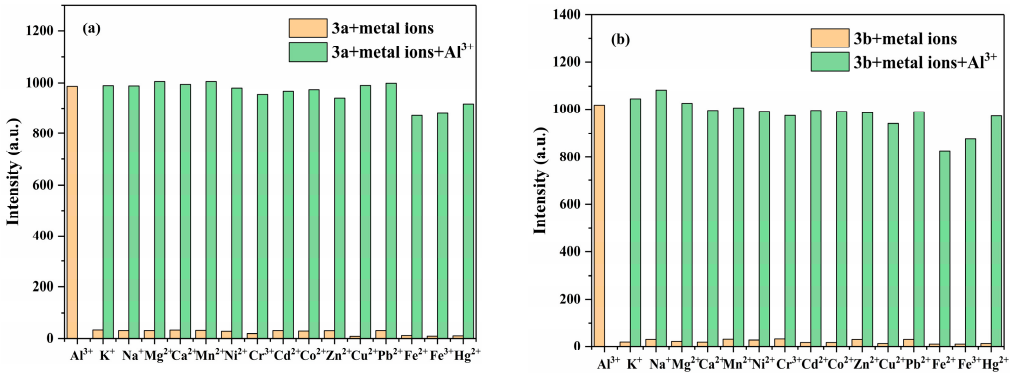



**Figure 8.** Fluorescence intensity of probe **3a** (**a**) and **3b** (**b**) (10 μM) with $Al^{3+}$ (10 eq.) and solutions after adding $Al^{3+}$ (10 eq.) ions upon the addition of various metal ions (10 eq.) in DMF/$H_2O$ ($v/v$ = 9:1) ($\lambda_{ex}$ = 405 nm for **3a** and $\lambda_{ex}$ = 400 nm for **3b**).

Similarly, as shown in Figure S5a, the fluorescence is enhanced when $Al^{3+}$ is added to compound **3c**, while the fluorescence intensity of the solution does not change significantly when other metal ions (excluding $Zn^{2+}$) are added. However, after continuing to add $Al^{3+}$, the fluorescence is enhanced. In addition, after adding $Al^{3+}$ to compound **3c** and continuing to add $Zn^{2+}$, the fluorescence intensity did not change significantly, indicating that the complex formed between compound **3c** and $Al^{3+}$ is more stable. Thus, other metal ions (including $Zn^{2+}$) have no significant interference with the detection of $Al^{3+}$ for compound **3c**.

Notably, as shown in Figure S5b, there is a difference in that the fluorescence is enhanced when $Zn^{2+}$ is added to compound **3c**, while the fluorescence intensity of the solution does not change significantly when other metal ions (excluding $Al^{3+}$) are added. After continuing to add $Zn^{2+}$, some solutions (previously added with $K^+$, $Na^+$, $Mg^{2+}$, $Ca^{2+}$, $Cu^{2+}$, $Mn^{2+}$, $Co^{2+}$, $Cd^{2+}$, $Ni^{2+}$ solutions) show the enhanced fluorescence. However, after adding $Zn^{2+}$ to the solution previously containing $Cr^{3+}$, $Hg^{2+}$, $Pb^{2+}$, $Fe^{2+}$, and $Fe^{3+}$, there is no significant change in the fluorescence of the solution. These indicate that the above-mentioned metal ions can interfere with the detection of $Zn^{2+}$ for compound **3c**.

### 2.4.3. Quantitative Identification of $Al^{3+}$ by Compounds **3a**–**3c**

Probes **3a**–**3c** exhibit excellent selectivity towards $Al^{3+}$. Furthermore, the fluorescence titration experiments were conducted on **3a**–**3c** for $Al^{3+}$, and the changes in fluorescence emission curves were analyzed. Once the fitting curves of the maximum emission intensity and ion concentration of the probe are plotted, and the limit of detection (LOD) can be calculated using the formula LOD = 3δ/K [56].

As shown in Figure 9a, with the increase of $Al^{3+}$ concentration from 0 to 15.0 eq., the fluorescence intensity at 509 nm increases with the increase of concentration. From Figure 9b, it can be observed that there is a good linear relationship between the fluorescence intensity of probe **3a** and the concentration of $Al^{3+}$ ($R^2$ = 0.999), and the LOD of probe **3a** for $Al^{3+}$ is calculated to be 3.14 × $10^{-7}$ M.

Similarly, as shown in Figure 9c, as the concentration of $Al^{3+}$ increases from 0 to 11.0 eq., the fluorescence intensity at 508 nm increases with the increase of the concentration. From Figure 9d, it can be observed that there is a good linear relationship between the fluorescence intensity of probe **3b** and the concentration of $Al^{3+}$ ($R^2$ = 0.999), and the LOD of probe **3b** for $Al^{3+}$ is calculated to be 2.81 × $10^{-7}$ M.

For probe **3c**, as shown in Figure S6a, when 0–12.0 eq. of $Al^{3+}$ is added to the solution of probe **3c**, there is a good linear relationship between the fluorescence intensity of probe **3c**

and the concentration of $Al^{3+}$ ($R^2$ = 0.996), and the LOD of probe **3c** for $Al^{3+}$ is calculated to be 2.86 × $10^{-7}$ M (Figure S6b).

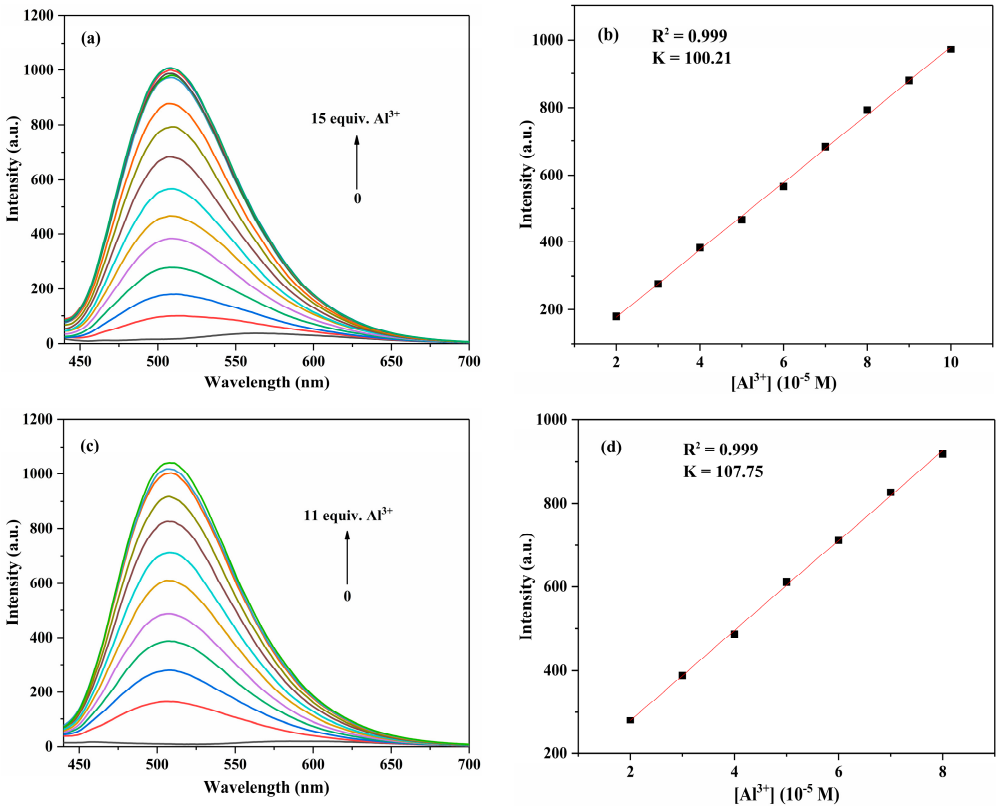



**Figure 9.** Fluorescence spectra of **3a** (**a**) and **3b** (**c**) in the presence of increasing amounts of $Al^{3+}$; Plot of fluorescence intensities of **3a** (**b**) and **3b** (**d**) respectively.

Notably, the LOD values of probes **3a**–**3c** are all lower than the maximum allowable concentration in drinking water specified by WHO [7]. In addition, when 0–1.0 eq. of $Zn^{2+}$ is added to probe **3c**, there is a good linear relationship between the fluorescence intensity and concentration of probe **3c** ($R^2$ = 0.991) (Figure S7a), and its LOD for $Zn^{2+}$ is calculated to be 8.64 × $10^{-9}$ M (Figure S7b).

Although probe **3c** can achieve nanomolar detection of $Zn^{2+}$, its detection of $Zn^{2+}$ is susceptible to interference, as mentioned above, so in the future, no further research will be conducted on the detection of $Zn^{2+}$.

### 2.4.4. Study on the Time Response of Probes **3a**–**3c** to $Al^{3+}$

The response speed of the probe to metal ions is an important factor in determining the real-time performance of the proposed fluorescence sensor [57]. Therefore, by rapidly adding 10.0 eq. of $Al^{3+}$ solution to the solution of probes **3a**–**3c** and testing their fluorescence intensity at different times, the relationship between the maximum fluorescence intensity of the probe and time was studied.

From Figure 10, it can be observed that after adding $Al^{3+}$ to the compound solution, the fluorescence intensity immediately increases and remains almost unchanged after 100 s. Meanwhile, the reaction times of probes **3b** and **3c** with $Al^{3+}$ are both 80 s, slightly faster than probe **3a** (90 s).

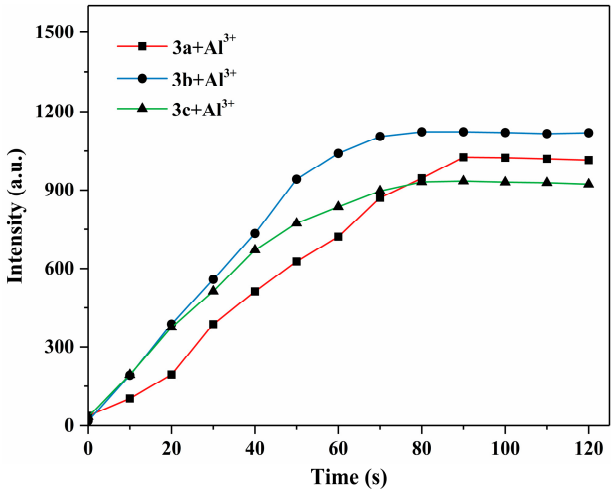



**Figure 10.** Time-dependent variation of maximum fluorescence intensity after the interaction between compound **3a**–**3c** and $Al^{3+}$.

Delightedly, the response times of probes **3a**–**3c** are shorter than most reported $Al^{3+}$ small molecule fluorescent probes [20,21,23] (please see Table S2 for a more detailed comparison). Therefore, the rapid response of compounds **3a**–**3c** to $Al^{3+}$ indicates that these three probes can be used for actual sample detection of $Al^{3+}$.

2.4.5. The Binding Ratio and Binding Constant of Probes **3a**–**3c** Interacting with $Al^{3+}$

In order to determine the binding ratio of $Al^{3+}$ to probes **3a**–**3c**, we conducted the continuous variation experiment to get Job's plot as the reported method [58]: fixing the total concentration of $Al^{3+}$ and ligands at 10 μM, changing the ratio of metal ions to ligands (0.1–0.9), and plotting the relationship between the maximum fluorescence intensity and the mole fraction of $Al^{3+}$. The value of the inflection point corresponds to the situation where $Al^{3+}$ is perfectly coordinated with the ligand.

As shown in Figure S8a, when the mole fraction of $Al^{3+}$ is 0.5, the Job plot shows a turning point, indicating that the binding stoichiometric ratio of probe **3a** to $Al^{3+}$ forming a complex is 1:1. Furthermore, the fluorescence titration data are linearly fitted by using the Benesi–Hildebrand equation, and the $K_a$ value can be calculated by using the intercept and slope of the line [59]. The binding constant between probe **3a** and $Al^{3+}$ is $6.53 \times 10^3$ M (Figure S8b). Similarly, as shown in Figure 11a, the maximum fluorescence intensity is achieved when the mole fraction of $Al^{3+}$ is 0.5, indicating that the stoichiometric ratio of probe **3b** to form a complex with $Al^{3+}$ is 1:1. The binding constant between probe **3b** and $Al^{3+}$ is $1.57 \times 10^4$ M (Figure 11b), which is higher than most reported $Al^{3+}$ small molecule fluorescent probes [20,29].

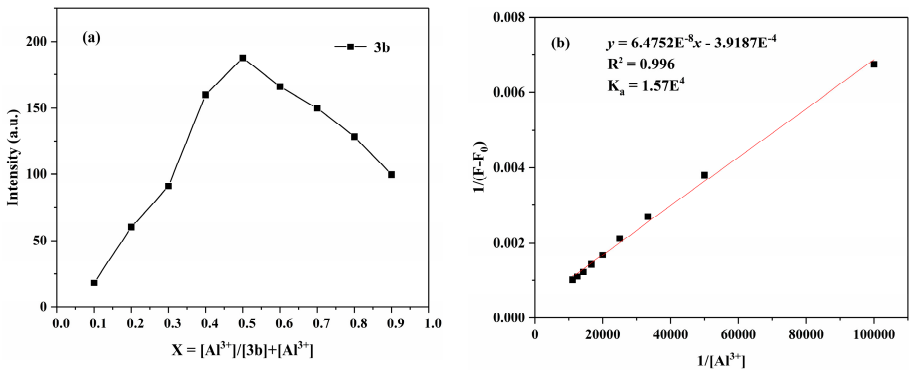



**Figure 11.** (**a**) The Job plot of **3b**-$Al^{3+}$; (**b**) the Benesi–Hildebrand plot of **3b**-$Al^{3+}$.

For probe **3c**, as shown in Figure S9a, the stoichiometric ratio of compound **3c** to $Al^{3+}$ binding is 1:1. In addition, the binding constant between compound **3c** and $Al^{3+}$ is $7.67 \times 10^3$ M (Figure S9b).

2.4.6. Study on pH Tolerance of Probes **3a**–**3c** in Interaction with $Al^{3+}$

It is well known that pH has a significant impact on the selectivity and sensitivity of the probes for metal ions [39]. Therefore, we measured and compared the maximum fluorescence intensity before and after the interaction between probes **3a**–**3c** solution and $Al^{3+}$ under different pH environments (Figure 12).

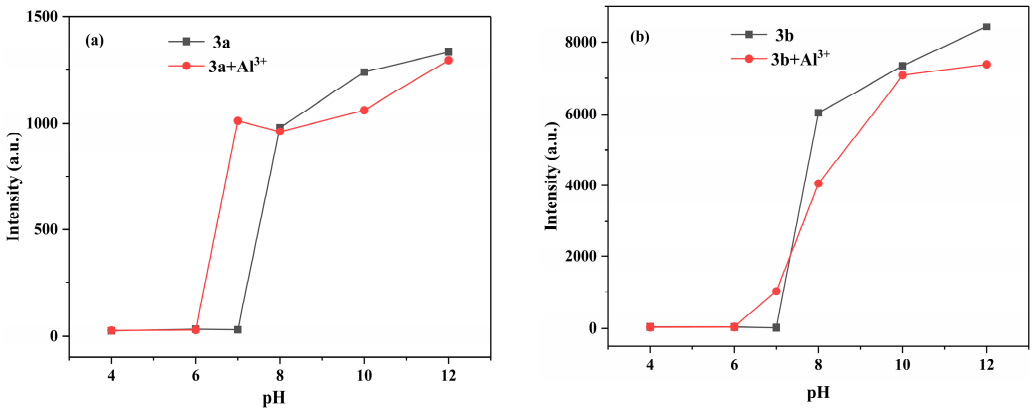



**Figure 12.** Different pH values of maximum fluorescence intensity before and after the interaction between compound **3a** (**a**)/**3b** (**b**) and $Al^{3+}$.

From Figure 12, it can be seen that probes **3a** and **3b** both have weak fluorescence intensity in the acidic range and cannot detect $Al^{3+}$. In other words, probes **3a** and **3b** can only detect $Al^{3+}$ under neutral conditions, also indicating that they can effectively detect the target ion under physiological conditions.

Interestingly, it also can be found that under alkaline conditions, both probes **3a** and **3b** exhibit strong fluorescence. Especially when the pH is 8, the fluorescence intensity of probes **3a** and **3b** will suddenly increase, and it will be enhanced by the increase of alkalinity. This may be due to the hydrolysis of compounds **3a** and **3b** under alkaline conditions [57], and the hydrolysis product 5-methyl salicylaldehyde also exhibits strong fluorescence under alkaline conditions. Especially for probe **3b**, there is also a noticeable color change under the naked eye (Figure S10). Therefore, probes **3a** and **3b** also can be considered as simple alkaline indicators with a mutation point pH of 8.

Differently, as shown in Figure S11, compound **3c** can detect $Al^{3+}$ under neutral and weakly alkaline conditions (no more than pH 8). Perhaps, due to the stronger alkalinity of probe **3c** compared to compounds **3a** and **3b**, it will not be hydrolyzed under the weakly alkaline condition.

However, it also can be found that compound **3c** exhibits strong fluorescence under strong alkaline conditions. When the pH is 9, the fluorescence intensity of compound **3c** suddenly enhances, and it will increase with increasing alkalinity (Figure S11). Thus, considering that probe **3c** also undergoes hydrolysis under strong alkaline conditions and exhibits strong fluorescence (Figure S10), it can also be considered a simple alkaline indicator with a mutation point pH of 9.

In addition, under acidic conditions, the fluorescence of probes **3a**–**3c** did not show significant changes before and after the addition of $Al^{3+}$, and all exhibited no fluorescence. This may be due to the weak fluorescence intensity of the probes caused by the hydrolysis of imine under acidic conditions.

### *2.5. Sensing Mechanism of Compounds* **3a–3c** *to* $Al^{3+}$

#### 2.5.1. $^1$H NMR and FT-IR Study on the Interaction Between Compounds **3a–3c** to $Al^{3+}$

From the previous Job's plot, it has been known that the stoichiometric ratio for the formation of complexes between compounds **3a–3c** and $Al^{3+}$ are all 1:1. In order to further understand the recognition mechanism of probes **3a–3c** for $Al^{3+}$, the studies of $^1$H NMR and Fourier transform infrared (FT-IR) spectroscopy (liquid film, using DMF as the solvent) were conducted [29].

The $^1$H NMR spectra of compounds **3a–3c** were tested in the absence and presence of $Al^{3+}$ (its nitrate) in DMSO-$d_6$. As shown in Figure 13, after the addition of $Al^{3+}$ to compound **3a**, the characteristic imine signal ($H_c$) at a chemical shift of 9.60 ppm is shifted to 10.20 ppm, and the amino proton ($H_a$) and phenolic hydroxyl proton ($H_b$) can not be observed, indicating that the N atom of the amino group, the O atom of the phenolic hydroxyl group, and the N atom of the imine all have participated in the coordination between compound **3a** and $Al^{3+}$ [39].

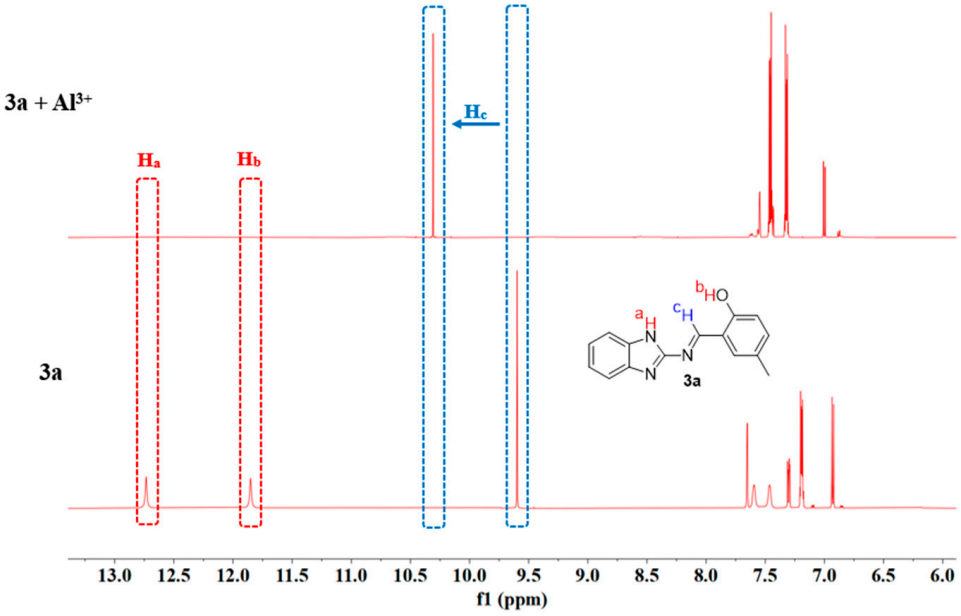



**Figure 13.** Hydrogen spectra of compound **3a** and **3a** + **Al**$^{3+}$.

Similarly, the binding modes of compounds **3b** and **3c** with $Al^{3+}$ can also be obtained through the $^1$H NMR titration experiments (as shown in Figures S12 and S14). Thus, the O atom of the phenolic hydroxyl group and the N atom of the imine in probes **3b** and **3c** can participate in the coordination of compounds **3b** and **3c** with $Al^{3+}$.

In the FT-IR spectrum of compound **3a** (Figure 14), there are peaks at 3430 $cm^{-1}$ (-OH) and 3312 $cm^{-1}$ (-NH), while they completely disappeared after the addition of $Al^{3+}$, indicating that the O atom in the phenolic hydroxyl group and the N atom in the amino group are involved in the binding of compound **3a** with $Al^{3+}$. At the same time, the strongest peak of C=N vibration at 1580 $cm^{-1}$ is weakened and shifted to 1695 $cm^{-1}$, indicating that the N atom in the imine group also participates in the binding with $Al^{3+}$ [16]. In addition, a new strong peak appears at 1344 $cm^{-1}$, which represents the stretching frequency of the $NO_3^-$ group [39].

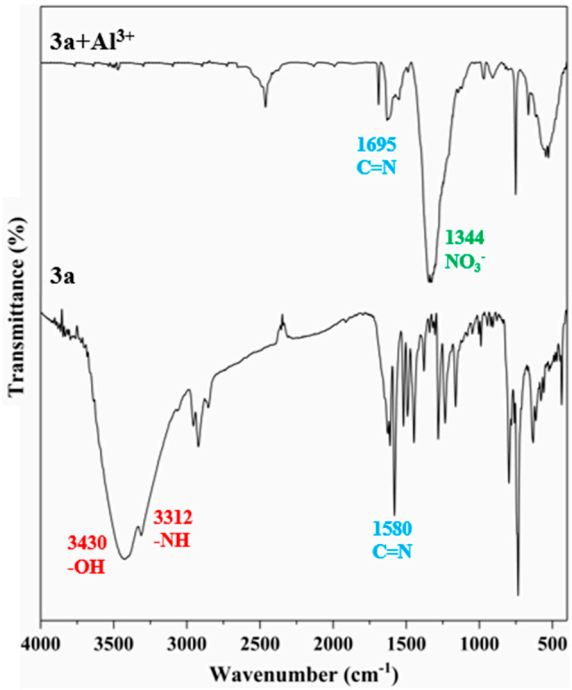



**Figure 14.** FT-IR spectra of compound **3a** and **3a** + $\mathbf{Al}^{3+}$.

As shown in Figures S13 and S15, the FT-IR spectra of compounds **3b** and **3c** also showed similar results.

2.5.2. DFT Study on the Interaction Between Compounds **3a**–**3c** to $Al^{3+}$

In order to further investigate the coordination interaction between probes **3a**–**3c** and $Al^{3+}$, DFT calculations were conducted on compounds **3a**-$Al^{3+}$, **3b**-$Al^{3+}$, and **3c**-$Al^{3+}$. The possible structures of compounds **3a**–**3c** and $Al^{3+}$ were geometrically optimized, and the LUMO-HOMO energy levels of **3a**-$Al^{3+}$, **3b**-$Al^{3+}$, and **3c**-$Al^{3+}$ were calculated [29].

As shown in Figure 15, probes **3a**–**3c** coordinate with $Al^{3+}$ in a stoichiometric ratio of 1:1. When probes **3a**–**3c** coordinate with $Al^{3+}$, the energy of HOMO is mainly distributed in the benzene ring and linker, while the energy of LUMO is mainly distributed near the aluminum atom (Figure 16).

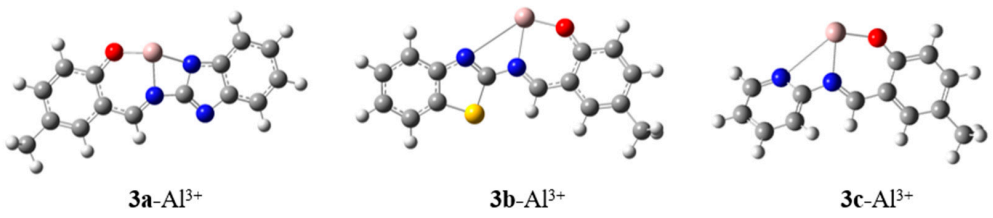



**Figure 15.** Optimized molecular structures of **3a**-$Al^{3+}$, **3b**-$Al^{3+}$, and **3c**-$Al^{3+}$.

After chelating with aluminum ions, probes **3a**–**3c** exhibit enhanced fluorescence intensity and spectral changes, known as chelation-enhanced fluorescence effect (CHEF) [3]. The CHEF effect significantly increases the fluorescence intensity [17], emitting bright yellow-green fluorescence. The energy gaps of **3a**-$Al^{3+}$, **3b**-$Al^{3+}$, and **3c**-$Al^{3+}$ are 2.72 eV, 2.46 eV, and 2.61 eV, respectively (Figure 16), which are significantly smaller than the energy gaps of compounds **3a**–**3c** ($\Delta E_{3a}$ = 3.56 eV, $\Delta E_{3b}$ = 3.48 eV, $\Delta E_{3c}$ = 3.76 eV). These indicate that compounds **3a**–**3c** tend to bind with $Al^{3+}$ and form more stable complexes [21,42,60]. The molecule's stiffness decreases non-radiative decay processes, further verifying that compounds **3a**–**3c** and $Al^{3+}$ "turn on" fluorescence through the CHEF effect.

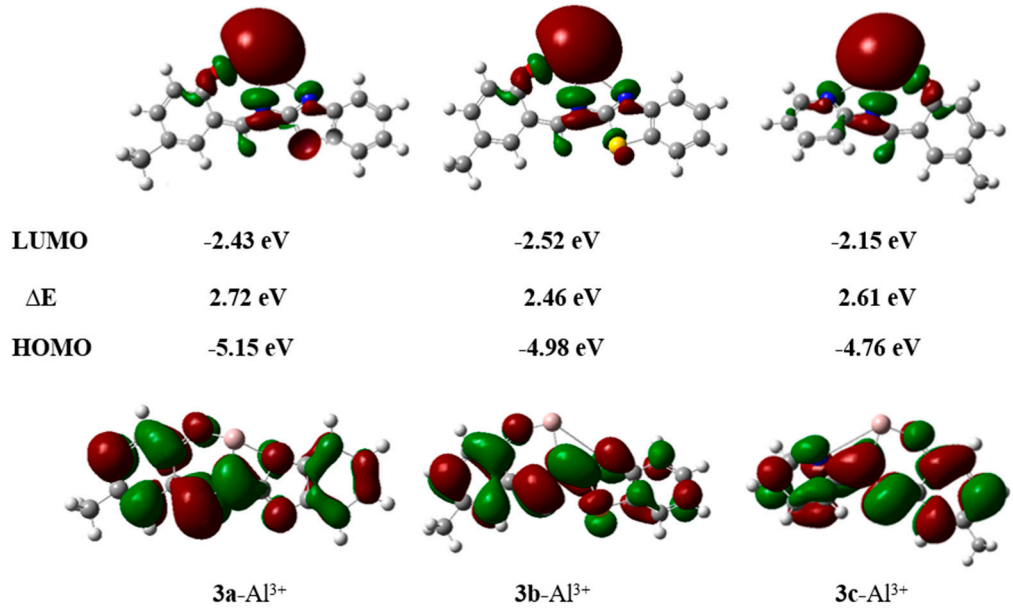
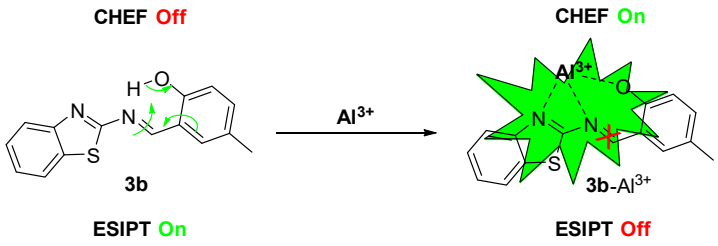



**Figure 16.** HOMO-LUMO energy level diagram of **3a**-$Al^{3+}$, **3b**-$Al^{3+}$, and **3c**-$Al^{3+}$.

In addition, compared with **3a**-$Al^{3+}$ and **3c**-$Al^{3+}$, **3b**-$Al^{3+}$ has the lowest energy gaps (Figure 16). This outcome finely explains why probe 3b can recognize $Al^{3+}$ with more obvious fluorescence changes and may correspond to the faster detection time [61].

At the same time, combining the $^1$H NMR and FT-IR tests has shown that when coordinating with $Al^{3+}$, the O atom of the phenolic hydroxyl group and the N atom of the imine both participate in the reaction, inhibiting the C=N isomerization and enhancing the rigidity of the probes after complexation with $Al^{3+}$, while the ESIPT effect was turned off and the CHEF effect was activated, resulting in fluorescence enhancement of the probe solution after the addition of $Al^{3+}$ [39]. Therefore, taking probe **3b** as an example with the best testing effect, the detection mechanism of probes **3a**-**3c** can be shown as Scheme 3.




**Scheme 3.** Proposed mechanism of compound **3b** for detection of $Al^{3+}$.

### *2.6. Practical Detection Application of Probes* **3a**–**3c** *to* $Al^{3+}$

#### 2.6.1. Application of Probes **3a**–**3c** in Detecting $Al^{3+}$ in Actual Water and Soil Samples

$Al^{3+}$ is prone to accumulate in water and soil samples, posing a serious threat to human health [7]. In order to evaluate the feasibility of probes **3a**–**3c** on $Al^{3+}$ in actual samples, we took distilled water, tap water, river water (the Pearl River water), and three actual water samples as well as soil samples as research objects (the geographical coordinates of all samples: latitude 23.052594° North and longitude 113.380105° East), and used the spiking method to conduct fluorescence emission spectrum test and fluorescence analysis to calculate the content of $Al^{3+}$ in the samples. The recovery rate and relative standard deviation (RSD) were determined through 3 parallel tests [60,62].

As shown in Figure S16, adding different concentrations (10 μM, 20 μM, 40 μM) of $Al^{3+}$ to different samples will gradually increase the fluorescence intensity of probe **3a** with

the increase of $Al^{3+}$ concentration. According to Table S3, the recovery range of probe **3a** for low concentration $Al^{3+}$ ($10^{-5}$ M) is 95.5–107%, with RSD less than 3.16%. These results indicate that probe **3a** exhibits high accuracy in identifying $Al^{3+}$ in actual samples and is suitable for detecting $Al^{3+}$ in actual water and soil samples.

Similarly, as shown in Figure 17, the fluorescence intensity of probe **3b** gradually increases with the increase of $Al^{3+}$ concentration. Meanwhile, according to Table 1, the recovery rate range of probe **3b** for low concentration $Al^{3+}$ ($10^{-5}$ M) is 98–105%, with RSD less than 3.09%. Therefore, these results indicate that probe **3b** is also suitable for detecting $Al^{3+}$ in actual water and soil samples.

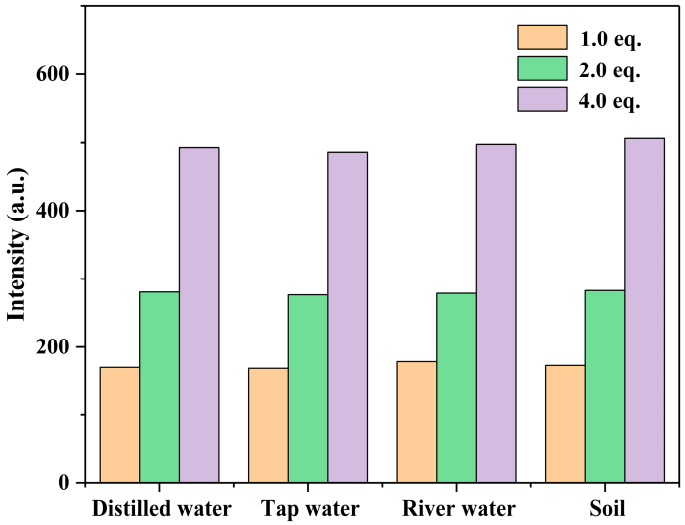



**Figure 17.** Relationship between the maximum fluorescence intensity of compound **3b** in different water and soil samples with different concentrations of $Al^{3+}$.

**Table 1.** Determination of $Al^{3+}$ in actual water and soil samples by compound **3b**.

| Samples | $Al^{3+}$ Added ($10^{-5}$ M) | $Al^{3+}$ Found ($10^{-5}$ M) | RSD (%, $n$ = 3) | Recovery (%) |
|---|---|---|---|---|
| Distilled water | 1 | 0.98 | 0.14 | 98 |
| | 2 | 1.99 | 1.53 | 99.5 |
| | 4 | 3.99 | 1.69 | 99.8 |
| Tap water | 1 | 0.97 | 0.88 | 97 |
| | 2 | 1.97 | 0.19 | 98.5 |
| | 4 | 3.92 | 2.34 | 98 |
| River water | 1 | 1.05 | 1.22 | 105 |
| | 2 | 1.99 | 3.09 | 99.5 |
| | 4 | 4.02 | 2.62 | 100.5 |
| Soil | 1 | 1.01 | 0.81 | 101 |
| | 2 | 2.03 | 2.30 | 101.5 |
| | 4 | 4.10 | 1.35 | 102.5 |
| Equation | y = 107.75x + 64.17 | | | |

In addition, the fluorescence intensity of probe **3c** is positively correlated with the concentration of $Al^{3+}$ (Figure S17), and the recovery range of compound **3c** for $Al^{3+}$ ($10^{-5}$ M) is 97–105%, with RSD less than 2.67% (Table S4). Therefore, these results indicate that probe **3c** is also suitable for detecting $Al^{3+}$ in actual water and soil samples.

In a word, compounds **3a–3c,** as three probes, are practical for detecting $Al^{3+}$ in actual water and soil samples.

2.6.2. Application of Test Strips Loaded with Compounds **3a**–**3c** for the Detection of $Al^{3+}$

The detection of metal ions through test strips has the advantages of convenience, simple operation, and low cost [44,63]. Therefore, in order to expand the practical applications of probes **3a**–**3c**, strip experiments were conducted [64,65] by cutting the Whatman filter paper into appropriate sizes, soaking them in DMF solution ($10^{-3}$ M) of compounds **3a**–**3c** for 10 min, and drying the test strips in an oven to prepare convenient test strips loaded with probes **3a**–**3c**.

Using one group as a blank control, different concentrations of $Al^{3+}$ solution ($10^{-2}$–$10^{-6}$ M) were added dropwise to the other five test strips. After drying with a hair dryer, the test strips were observed under a 365 nm UV lamp, as shown in Figure 18.

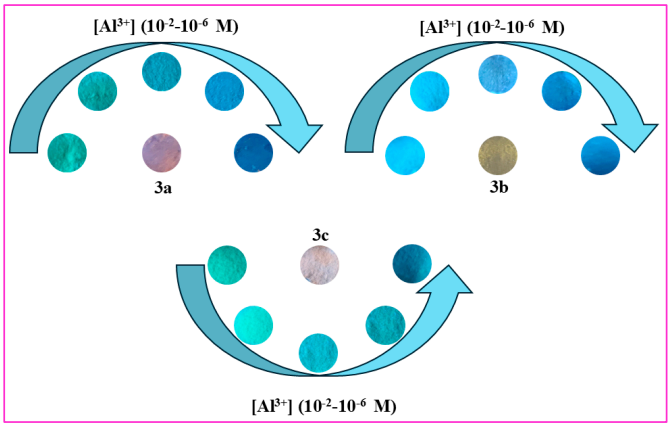



**Figure 18.** Application of probes **3a**–**3c** in test papers.

Obviously with the increase of $Al^{3+}$ concentration, the fluorescence of the test strips is changed significantly, from blue-green to blue fluorescence. Therefore, probes **3a**-**3c** can be made into test strips for convenient and intuitive detection of $Al^{3+}$.

## 3. Materials and Methods

### *3.1. Reagents and Instruments*

2-Aminobenzimidazole (**1a**), 2-aminobenzothiazole (**1b**), 2-aminopyridine (**1c**), and 5-methyl salicylaldehyde (**2**) were all purchased from Anhui Ze Sheng Technology Co., Ltd. (Shanghai, China). Whatman filter paper (110 mm) was purchased from Shanghai Bitai Biotechnology Co., Ltd. (Shanghai, China). All reagents and solvents used in this study are AR grade.

All fluorescence spectra were performed on an F-4600 fluorescence spectrometer (HITACGI Corporation, Tokyo, Japan). FT-IR spectroscopy was obtained using a Fourier transform infrared spectrometer (German Platinum Elmer Spectrum Two model, Ettlingen, Germany). The $^{1}H$ NMR and $^{13}C$ NMR spectra were tested on a 600 MHz Fourier transform nuclear magnetic spectrometer (Bruker AVANCE NEO 600M model, Ettlingen, Germany). Melting points were obtained on the WRX-4 micro melting point instrument (Shanghai Yimenshan Instrument and Equipment Co., Ltd., Shanghai, China). Mass spectrometry was tested on a liquid chromatography high-resolution mass spectrometer (Thermos Fisher Q Exactive, Waltham, MA, USA). X-ray single-crystal diffraction was tested using an X-ray single-crystal diffractometer (Agilent Gemini Model E, Santa Clara, CA, USA).

### *3.2. Synthesis*

3.2.1. Synthesis of Compound **3a**

For Scheme 2a, using the method described in reference [66], 2 mmol of 2-aminobenzimidazole (**1a**) and 2 mmol of 5-methyl salicylaldehyde (**2**) were dissolved into 10 mL

of anhydrous ethanol in a reaction flask. The reaction was carried out at 80 °C for 3 h. After the reaction was completed, the mixture was cooled to room temperature, giving solid precipitates. After filtration and washing with anhydrous ethanol, a solid crude product was obtained. Then, the further recrystallization with anhydrous ethanol gave the pure product **3a** as a yellow solid with a yield of 91%; m.p.: 235.0–235.5 °C; $^{1}$H NMR (600 MHz, DMSO-$d_6$), δ, ppm: 2.29 (s, 3H), 6.93 (*d*, *J* = 8.4 Hz 1H), 7.16–7.23 (m, 2H), 7.30 (*d*, *J* = 8.4 Hz, 1H), 7.46 (*d*, *J* = 8.4 Hz, 1H), 7.60 (*d*, *J* = 8.4 Hz, 1H), 7.66 (s, 1H), 9.60 (s, 1H), 11.84 (s, 1H), 12.73 (s, 1H), see Figure S18; $^{13}$C NMR (150 MHz, DMSO-$d_6$), δ, ppm: 19.92, 111.22, 116.74, 118.60, 119.09, 121.94, 122.26, 128.28, 131.80, 134.02, 135.54, 142.36, 154.06, 158.45, 165.25, see Figure S19; ESI-MS, *m*/*z* (%): Calcd for $C_{15}H_{14}N_3O([M + H]^+)$: 252.1131 (100), Found: 252.1126 (see Figure S20).

#### 3.2.2. Synthesis of Compound **3b**

For Scheme 2b, using the method described in reference [67], 2 mmol of 2-aminobenzothiazole (**1b**) and 2 mmol of 5-methyl salicylaldehyde (**2**) were dissolved into 5 mL of toluene in a reaction flask. After adding 30 μL of piperidine, the reaction was carried out at 110 °C for 3 h. Once the reaction was completed, the mixture was cooled to room temperature. After adding petroleum ether, there were solid precipitates. After filtration and washing with anhydrous ethanol, a solid crude product was obtained. Then, the further recrystallization with anhydrous ethanol gave the pure product **3b** as a yellow solid with a yield of 85% (51% [68]); m.p.: 131.0–132.4 °C; $^{1}$H NMR (600 MHz, DMSO-$d_6$), δ, ppm: 2.28 (s, 3H), 6.94 (*d*, *J* = 8.4 Hz, 1H), 7.33 (*d*, *J* = 8.4 Hz, 1H), 7.40–7.45 (m, 1H), 7.50–7.55 (m, 1H), 7.73 (s, 1H), 7.94 (*d*, *J* = 8.4 Hz, 1H), 8.07 (*d*, *J* = 8.4 Hz, 1H), 9.39 (s, 1H), 11.24 (s, 1H), see Figure S21; $^{13}$C NMR (150 MHz, DMSO-$d_6$), δ, ppm: 19.90, 116.86, 119.31, 122.39, 122.56, 125.24, 126.70, 128.54, 130.41, 133.94, 136.59, 151.25, 158.57, 165.53, 170.62 (see Figure S22).

#### 3.2.3. Synthesis of Compound **3c**

As Scheme 2c, 2 mmol of 2-aminopyridine (**1c**) and 2 mmol of 5-methyl salicylaldehyde (**2**) were dissolved into 10 mL of anhydrous ethanol in a reaction flask. The reaction was carried out at 80 °C for 1 h. After the reaction was completed, the mixture was cooled to room temperature, giving solid precipitates. After filtration and washing with anhydrous ethanol, a solid crude product was obtained. Then, the further recrystallization with anhydrous ethanol gave the pure product **3c** as an orange solid with a yield of 82% (63% [68]); m.p. 116.5–117.9 °C; $^{1}$H NMR (600 MHz, DMSO-$d_6$), δ, ppm: 2.28 (s, 3H), 6.90 (*d*, *J* = 8.4 Hz, 1H), 7.27 (*d*, *J* = 8.4 Hz, 1H), 7.33–7.39 (m, 1H), 7.44 (*d*, *J* = 7.8 Hz, 1H), 7.57 (s, 1H), 7.89–7.95 (m, 1H), 8.53 (*d*, *J* = 6.0 Hz, 1H), 9.43 (s, 1H), 12.73 (s, 1H), see Figure S23; $^{13}$C NMR (150 MHz, DMSO-$d_6$), δ, ppm: 19.91, 116.58, 118.71, 119.69, 122.84, 127.96, 132.80, 134.91, 139.01, 149.00, 157.69, 158.69, 164.26 (Figure S24).

### *3.3. Computational Details*

DFT and TD-DFT calculations were performed using Gaussian 09 D.01, and the structures of probes **3a**–**3c** before and after binding with $Al^{3+}$ were optimized at the B3LYP/6-31G (d) level. Then, their HOMO and LUMO were calculated at the B3LYP/6-31G (d, p) level, and the bandgap value was finally calculated [51,52].

### *3.4. Spectrophotometric Experiments*

Firstly, 1 mL of compound **3a**–**3c** solution with a concentration of $1.0 \times 10^{-2}$ M as the mother liquor was prepared and further diluted 1000 times during testing to prepare a test solution of compound **3a**–**3c** with a concentration of $1.0 \times 10^{-5}$ M. Then, serial 10 mL of metal nitrate solutions of $Al^{3+}$, $K^+$, $Na^+$, $Mg^{2+}$, $Ca^{2+}$, $Zn^{2+}$, $Cu^{2+}$, $Mn^{2+}$, $Co^{2+}$, $Cr^{3+}$, $Hg^{2+}$,

$Cd^{2+}$, $Ni^{2+}$, $Pb^{2+}$, $Fe^{2+}$, and $Fe^{3+}$ with the concentration of $1.0 \times 10^{-2}$ M were configured for use.

Fluorescence experiments were conducted to evaluate sensitivity by gradually increasing the concentration of target metal ions in the probe solution. In addition, in fluorescence measurement, the excitation wavelengths of compounds **3a**–**3c** are 405, 400, and 400 nm, respectively. The slit widths of both the excitation and emission were 5.0 nm. All the experiments were performed at room temperature.

## 4. Conclusions

Starting with 5-methylsalicylaldehyde, we designed and synthesized three Schiff base compounds **3a**–**3c** with different nitrogen heterocyclic fluorescent groups through a simple green reaction and characterized them by $^{1}$H NMR, $^{13}$C NMR, HRMS, and X-ray single crystal diffraction methods. Based on the coordination interaction between compounds **3a**–**3c** and $Al^{3+}$, compounds **3a**–**3c** have good selectivity for $Al^{3+}$ and can be used as fluorescent probes for detecting $Al^{3+}$. Thus, the properties of three fluorescent probes for $Al^{3+}$ were studied systematically for the first time by combining the theoretical calculations with the experimental observations.

Among them, probe **3b** with benzothiazole as the fluorescent group is the best, with a detection limit of $2.81 \times 10^{-7}$ M and a response time of 80 s. Notably, the LOD values of probes **3a**–**3c** are all below the maximum allowable concentration (7.41 μM) specified by WHO for drinking water. Furthermore, the mechanism of detecting $Al^{3+}$ with probes **3a**-**3c** has been elucidated through $^{1}$H NMR, FT-IR spectroscopy, and DFT calculation analysis. The theoretical research indicates that the energy gap of compound **3b** is the lowest of the three probes, resulting in its best results. Importantly, these probes **3a**–**3c** can be successfully applied for the practical detection of $Al^{3+}$ in water samples, soil samples, and test strips.

**Supplementary Materials:** The following supporting information can be downloaded at: https://www.mdpi.com/article/10.3390/molecules30051128/s1, Data of single-crystal X-ray analysis of compound **3a** (Table S1); Study on the optical properties of compounds **3a**–**3c** in different solvents (Figure S1); Study on the ACQ properties of compounds **3a** and **3b** (Figures S2 and S3); Selective study of compound **3c** with metal ions (Figure S4); Anti-interference study of compound **3c** with metal ions (Figure S5); Quantitative identification of $Al^{3+}$ by probe **3c** (Figures S6 and S7); Comparison of some fluorescent probes for $Al^{3+}$ (Table S2); The binding ratio and binding constant of compounds **3a** and **3c** interacting with $Al^{3+}$ (Figures S8 and S9); Study on pH tolerance of compounds **3a**–**3c** in interaction with $Al^{3+}$ (Figure S10 and S11); $^{1}$H NMR and FT-IR study on the interaction between compounds **3b** and **3c** to $Al^{3+}$ (Figures S12–S15); Application of compounds **3a** and **3c** in the detection of $Al^{3+}$ in actual samples (Figures S16 and S17, Tables S3 and S4); NMR Spectra and HRMS for compounds **3a**–**3c** (Figures S18–S24); See [2,15,20,21,23,26,27].

**Author Contributions:** Conceptualization, Z.-Y.W.; methodology, H.-Q.L.; formal analysis, H.-Q.L. and S.-H.Y.; data curation, Y.L. and W.-X.Y.; writing-original draft preparation, H.-Q.L., Z.-Y.L. and J.-Q.L.; writing-review and editing, H.-Q.L. and Z.-Y.W.; project administration, Z.-Y.W.; funding acquisition, Z.-Y.W. All authors have read and agreed to the published version of the manuscript.

**Funding:** This research was supported by NSFC (No. 20772035) and the Guangdong Basic and Applied Basic Research Foundation (No. 2021A1515012342).

**Institutional Review Board Statement:** Not applicable.

**Informed Consent Statement:** Not applicable.

**Data Availability Statement:** The original contributions presented in this study are included in the article/Supplementary Materials. Further inquiries can be directed to the corresponding author.

**Conflicts of Interest:** The authors declare no conflicts of interest.

## References


1. Meng, S.; Liu, J.X.; Yang, Y.Y.; Mao, S.; Li, Z. Lanthanide MOFs based portable fluorescence sensing platform: Quantitative and visual detection of ciprofloxacin and $Al^{3+}$. *Sci. Total Environ.* **2024**, *922*, 171115. [CrossRef]
2. Zou, Y.-L.; Liu, Y.-T. A novel isophorone-based NIR fluorescent and colormetric probe for $Al^{3+}$ sensing and its application for living cells and plants imaging. *Spectrochim. Acta A* **2024**, *312*, 124040. [CrossRef]
3. Sun, J.Q.; Wang, Y.G.; Wang, M.D.; Wang, H.M. A bisalicylhydrazone based fluorescent probe for detecting $Al^{3+}$ with high sensitivity and selectivity and imaging in living cells. *Spectrochim. Acta A* **2024**, *322*, 124784. [CrossRef]
4. Selvan, G.T.; Babu, L.; Enoch, I.M.V.; Srinivasadesikan, V.; Mariselvam, R.; Kumar, A.R.; Li, X.S.; Tang, P.J.; Selvakumar, P.M.; Zhang, Z. Surface-modified gold nanoparticles: A novel chemical probe for precise fluorescent detection of aluminium ($Al^{3+}$) ions; investigating DFT insights and molecular logic gate behaviour. *J. Mol. Liq.* **2024**, *397*, 124039. [CrossRef]
5. Yao, B.Y.; Zhang, J.H.; Han, M.; Liang, L.; Li, X.H.; Cai, X.H.; Leng, Y.L. Two novel "turn on" fluorescent probes for the determination of $Al^{3+}$ and its applications. *Inorg. Chim. Acta* **2023**, *153*, 110798. [CrossRef]
6. Che, H.C.; Tian, X.K.; Wang, J.H.; Dai, C.; Nie, Y.L.; Li, Y.; Lu, L.Q. A portable and intelligent logic detector for simultaneous and in-situ detection of $Al^{3+}$ and fluoride in groundwater. *J. Hazard. Mater.* **2023**, *458*, 131956. [CrossRef]
7. Zhou, L.-S.; Zhang, X.-Y.; Huang, Y. High selective, sensitive, reversible and imaging application sensor for aluminium detection. *J. Mol. Struct.* **2024**, *1310*, 138357. [CrossRef]
8. Mortada, W.I.; Alharthi, S. Preconcentration of aluminum by dual-cloud point extraction and its determination by inductively coupled plasma-optical emission spectrometry. *Curr. Anal. Chem.* **2021**, *17*, 1365–1372. [CrossRef]
9. Mashhadizadeh, M.H.; Amoli-Diva, M. Atomic absorption spectrometric determination of $Al^{3+}$ and $Cr^{3+}$ after preconcentration and separation on *3*-mercaptopropionic acid modified silica coated-$Fe_3O_4$ nanoparticles. *J. Anal. At. Spectrom.* **2013**, *28*, 251–258. [CrossRef]
10. Ham, Y.S.; Okazaki, M.; Suzuki, S.; Nakagawa, N. Determination of total aluminum concentration in soil solution using capillary electrophoresis. *Soil Sci. Plant Nutr.* **2003**, *49*, 9–16. [CrossRef]
11. Sharma, S.; Debnath, J.; Ghosh, K.S. Method for highly selective, ultrasensitive fluorimetric detection of $Cu^{2+}$ and $Al^{3+}$ by Schiff bases containing o-phenylenediamine and o-aminophenol. *Methods* **2023**, *217*, 27–35. [CrossRef]
12. Yang, K.; Shi, S.B.; Han, S.L.; Wu, J.Y.; Li, S.C.; Zhu, R.; Tai, S.D.; Zhang, K. Europium-macrocycle based lab-on-a-molecule fluorescent probe and its multianalyte detection of phosphate and aluminum ions. *Sens. Actuators B* **2024**, *410*, 135734. [CrossRef]
13. Zhang, Y.; Wang, G. A novel ethylene linkage-based covalent organic framework for turn-on fluorescence sensing for $Al^{3+}$ with excellent selectivity and sensitivity. *Int. J. Biol. Macromol.* **2024**, *262*, 130195. [CrossRef]
14. Ma, L.; Xia, B.Y.; Zhang, Y.Y.; Lv, J.X.; Lv, Y.G.; Zhang, X.Y. A highly sensitive fluorescent probe for the detection of $Al^{3+}$ and study of its practical application. *J. Mol. Liq.* **2024**, *1316*, 138886. [CrossRef]
15. Hu, Y.; Lu, L.M.; Wu, Y.X.; Li, Y.J.; Wang, F.; Chen, X.Q.; Fu, H.Y.; She, Y.B. Bifunctional ratiometric fluorescent membrane containing pyrene-based probe for visual monitoring and efficient removal of $Al^{3+}$. *Sens. Actuators B* **2024**, *413*, 135860. [CrossRef]
16. Liu, Y.C.; Li, N.; Zhang, Y.L.; Wang, Y. Diphenyl imidazole-based fluorescent chemosensor for $Al^{3+}$ and its $Al^{3+}$ complex toward water detection in food products. *Food Chem.* **2023**, *420*, 136138. [CrossRef]
17. Li, M.; Li, N.; Shao, F.; Wang, R.; Chen, M.; Liu, Y.-J.; Zhao, Y.; Li, R. Synthesis of a super-low detection limit fluorescent probe for $Al^{3+}$ and its application in fluorescence imaging of zebrafish and cells. *Spectrochim. Acta A* **2024**, *308*, 123676. [CrossRef]
18. Bhiri, F.; Chemli, M.; Sakly, N.; Bahrouni, Y.; Wazzan, N.; Majdoub, M. New chromogenic and fluorogenic symmetric carbazole Schiff base-derivative: Synthesis, sensing performances and smartphone-assisted fluorometric assay for selective $Al^{3+}$ detection in drinking water. *J. Mol. Struct.* **2025**, *1322*, 140548. [CrossRef]
19. Lei, X.L.; Zou, Y.Y.; Liang, Q.J.; Xu, W.S.; Lao, S.S.; Yang, B.; Li, L.G.; Yang, L.T.; Liu, H.; Ma, L.J. An ultrasensitive *4*-(diethylamino) salicylaldehyd-based fluorescence enhancement probe for the detection of $Al^{3+}$ in aqueous solutions and its application in cells. *J. Photochem. Photobiol. A* **2022**, *428*, 113854. [CrossRef]
20. Yasar, O.G.; Elmas, S.N.K.; Aydin, D.; Arslan, F.N. $Al^{3+}$ selective ratiometric fluorescent and colorimetric chemoprobe and its practical applications in foods, test kits and smartphone. *J. Photochem. Photobiol. A* **2024**, *447*, 115238.
21. Wang, S.; Liao, Y.H.; Feng, H.J.; Wu, L.Y.; He, W.Y. The studies on a fluorescent probe of Schiff base modified by 1,2,3-triazole to detecting $Al^{3+}$ and living cell imaging. *J. Mol. Struct.* **2024**, *1296*, 136730. [CrossRef]
22. Wang, X.M.; Li, Y.F.; Liu, L.Q.; Tan, Z.Q.; Zhou, X.H.; You, Y.J.; Wang, S. A dual-emission fluorescence coordination polymer for simultaneous quantification of $Al^{3+}$ and $Pb^{2+}$ in their mixtures. *J. Mater. Chem. C* **2024**, *12*, 17144–17152. [CrossRef]
23. Zhao, C.; Xu, H.M.; Meng, Y.T.; Wang, Y.; Shuang, S.M.; Dong, C. Anthraquinone-based Schiff base fluorescent probe for the sequential sensing of $Al^{3+}$ and pyrophosphate in a near-perfect aqueous solution and bioimaging. *J. Mol. Liq.* **2023**, *391*, 123326. [CrossRef]
24. Suganthi, G.; Ajitha, R.; Babu, A.A.; Kamalesu, S.; Subramanian, R.; Arun, T.; Godlyn, A.; Nagaraj, K. Highly efficient fluorescence sensing of $Al^{3+}$ ions using a sensitive carbazole based Schiff base. *Inorg. Chim. Acta* **2024**, *161*, 112150. [CrossRef]

25. Zhang, Z.Y.; Wang, S.; Wang, M.X.; Li, H.M.; Liang, Q.J.; Tang, J.W.; Sun, J.; Ma, L.J.; Liu, H. An ultra-sensitive fluorescence multi-channel and colorimetric probe based on salicylaldehyde hydrazone for $Al^{3+}$ recognition with a 3:1 binding ratio. *J. Mater. Chem. C* **2024**, *12*, 15144–15151. [CrossRef]
26. Dev, K.; Singh, S.; Bhardwaj, S.; Kukreti, P.; Ramakanth, D.; Kumar, P.; Saini, S.; Roy, P.; Srivastava, V.C.; Ghosh, K.; et al. Solvent-selective fluorescence sensing of $Mg^{2+}$ and $Al^{3+}$ ions by pincer-type NNO Schiff base ligand: An experimental and DFT optimized approach. *Chem.-Eur. J.* **2024**, *30*, e202403256. [CrossRef]
27. Islam, M.S.; Hoque, A.; Baig, K.M.Y.; Sarmin, M.; Kole, G.K.; Hoda, M.; Alam, M.A. A zwitterionic probe for ratiometric fluorescent detection of aluminium(III) ion in aqueous medium and its application in bioimaging. *Spectrochim. Acta A* **2024**, *311*, 124005. [CrossRef]
28. Goswami, N.; Naithani, S.; Goswami, T.; Kumar, P.; Kumar, S. A quinoline derived Schiff base as highly selective 'turn-on' probe for fluorogenic recognition of $Al^{3+}$ ion. *Spectrochim. Acta A* **2024**, *310*, 123971. [CrossRef]
29. Elmas, S.N.K.; Boran, T.; Arslan, F.N.; Özhan, G.; Erdemir, S. Ultrafast and nanomolar detection of $Al^{3+}$: Furazan based fluorescent chemosensor and its practices in smartphone, test kit, water samples and living-cell. *Microchem. J.* **2024**, *200*, 110444. [CrossRef]
30. Jiang, Q.; Song, J.; Yang, X.Q.; Rao, X.P.; Zhao, P.; Wang, Z.L. A novel reversible fluorescent probe for sequential detection of $Al^{3+}$ and $HPO_4^{2-}$ based on caffeic acid and its applicability in cell imaging. *Spectrochim. Acta A* **2024**, *307*, 123627. [CrossRef]
31. Chen, S.-H.; Jiang, K.; Xiao, Y.; Cao, X.-Y.; Arulkumar, M.; Wang, Z.-Y. Recent endeavors on design, synthesis, fluorescence mechanisms and applications of benzazole-based molecular probes toward miscellaneous species. *Dyes Pigm.* **2020**, *175*, 108157. [CrossRef]
32. Chen, S.-H.; Jiang, K.; Liang, Y.-H.; He, J.-P.; Xu, B.-J.; Chen, Z.-H.; Wang, Z.-Y. Fine-tuning benzazole-based probe for the ultrasensitive detection of $Hg^{2+}$ in water samples and seaweed samples. *Food Chem.* **2023**, *428*, 136800. [CrossRef]
33. Wang, R.Y.; Feng, X.; Feng, B.Y.; Chen, Y. Boron-mediated one-pot access to salicylaldehydes via *ortho*-C-H hydroxylation of benzaldehydes. *RSC Adv.* **2024**, *14*, 19922–19925. [CrossRef]
34. Mohammed, A.K.; Pandikassala, A.; Sánchez, P.P.; Gaber, S.A.; Canossa, S.; Kurian, M.; Xavier, G.; He, Y.; Gándara, F.; Kurungot, S.; et al. Iron salicylaldehydate conjugated metal-organic framework for quasi solid-state supercapacitor. *Chem. Eng. J.* **2024**, *496*, 153589. [CrossRef]
35. Mandi, A.; Bar, N.; Biswas, D.; Ray, A.; Ghosh, K.; Mondal, D.; Das, G.K.; Chowdhury, P. Rhodamine 6G salicylaldehyde hydrazone-Zn complex: Synthesis, characterization, photochromism, understanding, and application. *J. Lumin.* **2024**, *271*, 120611. [CrossRef]
36. Sahu, M.; Ganguly, M.; Sharma, P. Recent applications of coinage metal nanoparticles passivated with salicylaldehyde and salicylaldehyde-based Schiff bases. *Nanoscale Adv.* **2024**, *6*, 4545–4566. [CrossRef] [PubMed]
37. Rajalakshmi, K.; Muthusamy, S.; Lee, H.J.; Kannan, P.; Zhu, D.W.; Song, J.W.; Nam, Y.S.; Heo, D.N.; Kwon, I.; Luo, Z.B.; et al. Dual-channel fluorescent probe for discriminative detection of $H_2S$ and $N_2H_4$: Exploring sensing mechanism and real-time applications. *J. Hazard. Mater.* **2024**, *465*, 133036. [CrossRef]
38. Zhou, N.; Cai, M.Y.; Zheng, S.N.; Guo, H.Y.; Yang, F.F. First organic fluorescent sensor for pesticide paclobutrazol based on tetraphenylimidazole Schiff base. *Sens. Actuators B* **2024**, *417*, 136051. [CrossRef]
39. Dathees, T.J.; Narmatha, G.; Prabakaran, G.; Seenithurai, S.; Chai, J.D.; Kumar, R.S.; Prabhu, J.; Nandhakumar, R. Salicylaldehyde built fluorescent probe for dual sensing of $Al^{3+}$, $Zn^{2+}$ ions: Applications in latent fingerprint, *bio*-imaging & real sample analysis. *Food Chem.* **2024**, *441*, 138362.
40. Palta, A.; Kumar, G.; Paul, K.; Luxami, V. Highly selective colorimetric and fluorescent probe for $F^-$ and $P_2O_7^{4-}$ based on AIEE and dual ESIPT. *J. Mol. Struct.* **2024**, *1316*, 138880. [CrossRef]
41. Dwivedi, S.K.; Arachchige, D.L.; Vohs, T.; Tang, J.N.; Usimaki, K.; Olowolagba, A.M.; Fritz, D.R.; Luck, R.L.; Werner, T.; Liu, H.Y. Near-infrared rhodol dyes bearing salicylaldehyde moieties for ratiometric pH sensing in live cells during mitophagy and under hypoxia conditions. *J. Mater. Chem. B* **2023**, *11*, 2852–2861. [CrossRef] [PubMed]
42. Yang, Y.-Y.; Ma, P.-Y.; Xue, J.-H.; Yang, D.-D.; Shi, Y.-S.; Zhao, X.; Ma, Q. A highly selective fluorescent probe based on multi-binding site hydrazone chemosensor for $Al^{3+}$ detection. *Microchem. J.* **2024**, *200*, 110495. [CrossRef]
43. Pang, Y.L.; Meng, D.S.; Liu, J.; Duan, S.X.; Fan, J.R.; Gao, L.Y.; Long, X.S. Schiff base compounds as fluorescent probes for the highly sensitive and selective detection of $Al^{3+}$ ions. *Molecules* **2023**, *28*, 3090. [CrossRef] [PubMed]
44. Zhao, J.N.; Li, C.Q.; Wei, S.H.; Lu, C.W.; Zou, L.W. A multifunctional fluorescent probe based on Schiff base with AIE and ESIPT characteristics for effective detections of $Pb^{2+}$, $Ag^+$ and $Fe^{3+}$. *Spectrochim. Acta A* **2023**, *300*, 122904. [CrossRef]
45. Duan, N.; Ding, L.Y.; Yang, S.X.; Tian, H.Y.; Sun, B.G. A benzimidazole-based 'turn-on' fluorescent probe for highly sensitive detection of $Fe^{3+/2+}$: Synthesis, performance, DFT calculations and applications. *J. Mater. Chem. C* **2024**, *12*, 7359–7365. [CrossRef]
46. Liu, Y.L.; Li, L.; Yue, M.L.; Yang, L.; Sun, F.; Xu, G.Q.; Fu, Y.; Ye, F. A switch-on fluorescent probe for detection of mesotrione based on the straightforward cleavage of carbon-nitrogen double bond of Schiff base. *Chem. Eng. J.* **2022**, *430*, 132758. [CrossRef]
47. Wang, X.Y.; Shu, J.; Ni, T.; Xu, C.X.; Tang, J.Y.; Xu, B.; Liu, X.Q.; Zhang, K.M.; Jiang, W.D. Multiple stimuli-responsive properties of coumarin-salicylaldehyde Schiff bases. *Dyes Pigm.* **2023**, *208*, 110820. [CrossRef]

48. Soliman, A.I.A.; Sayed, M.; Elshanawany, M.M.; Younis, O.; Ahmed, M.; El-Dean, A.M.K.; Abdel-Wahab, A.M.A.; Wachtveitl, J.; Braun, M.; Fatehi, P.; et al. Base-free synthesis and photophysical properties of new Schiff bases containing indole moiety. *ACS Omega* **2022**, *7*, 10178–10186. [CrossRef]
49. Lu, C.X.; Xu, J.W.; Song, Z.; Dai, Z.Y. Advancements in ESIPT probe research over the past three years based on different fluorophores. *Dyes Pigm.* **2023**, *208*, 110820. [CrossRef]
50. Yang, M.; Mu, H.Y.; Gao, J.A.; Zhen, Q.; Wang, X.N.; Guan, X.T.; Li, H.; Li, B. Screening the optimal probe by expounding the ESIPT mechanism and photophysical properties in vis-HBX with multimodal substitutions. *Molecules* **2023**, *28*, 3090.
51. Zhao, C.; Aziz, A.; Lu, W.J.; Xu, H.M.; Asif, M.; Shuang, S.M.; Dong, C. A turn-on anthraquinone-derived colorimetric and fluorometric dual-mode probe for highly selective $Hg^{2+}$ determination and bioimaging in living organisms. *J. Hazard. Mater.* **2024**, *479*, 135694. [CrossRef] [PubMed]
52. Anan, J.; Fosu, E.A.; Obuah, C.; Ainooson, M.K.; Aniagyei, A.; Hamenu, L.; Oppong, A.; Muller, A. A DFT and TD-DFT studies of the photosensitizing capabilities of thiophene-based dyes. *Comput. Theor. Chem.* **2024**, *1237*, 114633. [CrossRef]
53. Zhao, J.; Li, Q.; Guo, M.L.; Yan, L.; Hu, G.X.; Zhu, L.X.; Yin, H.; Shi, Y. Solvent effects on the ESIPT emission of salicylaldehyde Schiff base derivative: A theoretical reconsideration. *J. Mol. Liq.* **2024**, *408*, 125265. [CrossRef]
54. Queiroz, M.H.; Alves, T.V.; Rivelino, R.; Canuto, S. Influence of solvents and halogenation on ESIPT of benzimidazole derivatives for designing turn-on fluorescence probes. *ACS Omega* **2024**, *9*, 22102–22111. [CrossRef] [PubMed]
55. Zhang, Z.C.; Liu, C.; Lu, Y.; Zhao, W.L.; Zhu, Q.G.; He, H.S.; Chen, Z.J.; Wu, W. In vivo fluorescence imaging of nanocarriers in near-infrared window II based on aggregation-caused quenching. *J. Nanobiotechnol.* **2024**, *22*, 488. [CrossRef]
56. Jiang, K.; Chen, S.-H.; Luo, S.-H.; Pang, C.-M.; Wu, X.-Y.; Wang, Z.-Y. Concise design and synthesis of water-soluble fluorescence sensor for sequential detection of Zn(II) and picric acid via cascade mechanism. *Dyes Pigm.* **2019**, *167*, 164–173. [CrossRef]
57. Sidqi, M.E.; Aziz, A.A.A.; Abolehasan, A.E.; Sayed, M.A. Photochemical processing potential of a novel Schiff base as a fluorescent probe for selective monitoring of $Al^{3+}$ ions and bioimaging in human cervical cancer HeLa cells. *J. Photochem. Photobiol. A* **2022**, *424*, 113616. [CrossRef]
58. Zhao, C.; Xu, H.M.; Zhang, X.R.; Meng, Y.T.; Shuang, S.M.; Dong, C. Anthraquinone-metal complex fluorescence sensing platform for monitoring PPi mediated by $Al^{3+}$ and bioimaging. *J. Mol. Struct.* **2024**, *1308*, 138022. [CrossRef]
59. Sultana, T.; Mahato, M.; Tohora, N.; Ahamed, S.; Das, S.K. An azine-based chromogenic, fluorogenic probe for specific cascade detection of $Al^{3+}$ and $PO_4^{3-}$ ions. *J. Photochem. Photobiol. A* **2023**, *444*, 114951. [CrossRef]
60. Xing, Z.Y.; Wang, J.L.; Huang, J.H.; Chen, X.F.; Zong, Z.A.; Fan, C.B.; Huang, G.M. A significant fluorescence turn-on probe for the recognition of $Al^{3+}$ and its application. *Molecules* **2022**, *27*, 2569. [CrossRef]
61. Li, L.; Zhao, J.N.; Lue, C.W. ESIPT performance bis-Schiff base for multifunctional detection of $Pb^{2+}$, $Mg^{2+}$ and $Al^{3+}$ ions through "turn-on" response and its biological application. *Res. Chem. Intermed.* **2024**, *50*, 5017–5038. [CrossRef]
62. Chen, Z.-H.; Chen, Z.-J.; Zeng, Y.; Liang, Y.-T.; Guo, J.-L.; Yang, S.-H.; Wang, Z.-Y. Multifunctional *N*-fused fluorescent probes for detection of iron ions and nitro explosives. *Spectrochim. Acta A* **2025**, *326*, 125281. [CrossRef] [PubMed]
63. Mishra, S.; Mamidi, P.; Chattopadhyay, S.; Singh, A.K. Economically viable multi-responsive probes for fluorimetric detection of trace levels of $Ga^{3+}$, $Al^{3+}$ and PPi in near aqueous medium. *J. Photochem. Photobiol. A* **2023**, *434*, 114225. [CrossRef]
64. Zhao, L.-X.; He, X.-L.; Xie, K.-B.; Hu, J.-J.; Deng, M.-Y.; Zou, Y.-L.; Gao, S.; Fu, Y.; Ye, F. A novel isophorone-based fluorescent probe for recognition of $Al^{3+}$ and its bioimaging in cells and plants. *Spectrochim. Acta A* **2023**, *385*, 121882. [CrossRef] [PubMed]
65. Chen, Z.-H.; Chen, Z.-J.; Li, W.-X.; Zeng, Y.; Lin, J.-Q.; Tao, G.-S.; Wang, Z.-Y. Synthesis of a novel *N*-fused ring based organic molecule probe and its detection of iron. *Inorg. Chim. Acta* **2024**, *163*, 112381. [CrossRef]
66. Pan, W.Y.; Yang, X.Y.; Wang, Y.S.; Wu, L.; Liang, N.; Zhao, L.S. AIE-ESIPT based colorimetric and "OFF-ON-OFF" fluorescence Schiff base sensor for visual and fluorescent determination of $Cu^{2+}$ in an aqueous media. *J. Photochem. Photobiol. A* **2021**, *420*, 113506. [CrossRef]
67. Sayed, M.; Kamal, A.M.; Ahmed, M.M.; Hassanien, R. Synthesis of some new heterocyclic compounds containing indole moiety. *Eur. Chem. Bull.* **2017**, *6*, 171–176. [CrossRef]
68. Jia, W.G.; Zhang, H.; Zhang, T.; Xie, D.; Ling, S.; Sheng, E.H. Half-sandwich ruthenium complexes with Schiff-base ligands: Syntheses, characterization, and catalytic activities for the reduction of nitroarenes. *Organometallics* **2016**, *35*, 503–512. [CrossRef]


**Disclaimer/Publisher's Note:** The statements, opinions and data contained in all publications are solely those of the individual author(s) and contributor(s) and not of MDPI and/or the editor(s). MDPI and/or the editor(s) disclaim responsibility for any injury to people or property resulting from any ideas, methods, instructions or products referred to in the content.